

A Three-Dimensional-Printed Soft Robotic Glove With Enhanced Ergonomics and Force Capability

Juan Yi, *Student Member, IEEE*, Xiaojiao Chen, *Student Member, IEEE*, and Zheng Wang, *Senior Member, IEEE*

Abstract—This letter presents a novel soft robotic glove system for assistive and rehabilitative applications, offering a powerful, low-profile, and convenient solution for the growing elderly and patient population. The low-profile soft glove worn by the user weighs below 50 g, providing cable-driven flexion and extension actuations independently for all five fingers without any rigid joint or linkage, and therefore does not require joint alignment or custom fitting. Novel bidirectional linear soft actuators are developed to drive each finger with enhanced payload and improved user comfort. The actuators are regulated by novel soft orifice valves developed to provide airflow control using soft material deformation. The design, modeling, and fabrication procedure of the entire soft glove system is presented in detail. The system comprises entirely of three-dimensional (3-D) printed and commercially available components, it is therefore repeatable by anyone with access to a consumer-grade 3-D printer. The fabricated components and glove system were evaluated in a series of validation experiments. The lightweight and compliant soft glove could achieve full-range finger motion and forces up to 40 N at the fingertip with actuation pressure as low as 60 kPa, making the system capable for most grasping and interaction tasks in healthcare, service, as well as edutainment applications.

Index Terms—Soft actuator, soft glove, soft robot, wearable device.

I. INTRODUCTION

ASSISTIVE robotic gloves received increasing research attention in recent years, with global aging and the rising number of patients with impaired hand functions, requiring hand motion assistance and rehabilitation [1]. To partially or completely replace human hand motoring functions, conventional robotic assistive devices apply external forces to move the fingers with rigid exoskeletons actuated by electric motors [3], [4]. To match the high dexterity of human hand motion and

different sizes of hands, such rigid robotic devices generally require high degrees of customization and calibration. And controller sophistication is unavoidable to ensure interaction safely. In order to improve the ergonomics design and promote at-home usage of robotic gloves, there have been efforts in weight reduction by means of cable transmission [5], placing electric motors remotely from the user. Fluid-driven soft material robotic actuators have also been adopted in glove-type applications for their inherent compliance and safety [6]–[10]. Although compliance could also be achieved by modifications of conventional motors, such as Serial Elastic Actuators [11], soft actuators are favorable in wearable applications due to their light weight, and low production cost.

Different types of soft actuators could be either attached directly (bending type) to the back of hand [6], or mounted on an off-hand console (linear type) and drive the fingers by cable transmission [8]. With their excellent compliance and conformity, soft robotic gloves generally do not require precise calibration and customization, but could achieve superior ergonomics compared to rigid exoskeletons in activities of daily living (ADLs). With the simple structure and easy fabrication procedure of soft actuators, there have been efforts towards open-source soft robots for the general public [12], [13]. On the other hand, the limited structural stiffness of soft bending actuators restricted the force capability of direct-mounting soft gloves. For linear soft actuators, such as the McKibben-type actuators often found in wearable devices [8], [14], the actuator performance limitations, both in the motion range and force output profile, are often restricting the overall system characteristics, hence limiting their real-world applications.

In this letter, we propose a 3-D printable soft robotic glove system with enhanced ergonomics, large force capability and low actuation pressure. The whole system, as illustrated in Fig. 1, comprising of the soft glove, bidirectional linear soft actuator (BLSA) and soft orifice valves (SOV), are fabricated with soft materials. By utilizing soft materials and actuated with compressed air, the robotic glove system exhibits performance in grasping daily objects with an actuator could generate 180 N forces with pressure as low as 100 kPa. Force transmitted to the fingertip is up to 40 N in 60 kPa actuation pressure. All structural components of the proposed robotic glove are fabricated with 3D-printed soft materials, achieving both high accessibility and low fabrication cost. In addition, designs of the proposed novel BLSA and the SOV are also presented. The performance of the proposed system is validated by experimental results using the fabricated glove.

Manuscript received February 15, 2017; accepted July 10, 2017. Date of publication August 8, 2017; date of current version August 25, 2017. This letter was recommended for publication by Associate Editor G. Salvietti and Editor Y. Yokokohji upon evaluation of the reviewers' comments. This work was supported in part by the Hong Kong RGC-ECS Grant 27210315, in part by the HKU Seed Funding for Basic Research 201511159051, and in part by the Shenzhen Science and Technology Fund for Basic Research JCYJ20150629151046885. (Corresponding author: Zheng Wang.)

J. Yi and Z. Wang are with the Department of Mechanical Engineering, The University of Hong Kong, Hong Kong, and also with the HKU Shenzhen Institute of Research and Innovation (HKU-SIRI), Shenzhen 999077, China (e-mail: yijuan@connect.hku.hk; zwangski@hku.hk).

X. Chen is with the Department of Mechanical Engineering, The University of Hong Kong, Hong Kong (e-mail: yii402072495@gmail.com).

Digital Object Identifier 10.1109/LRA.2017.2737481

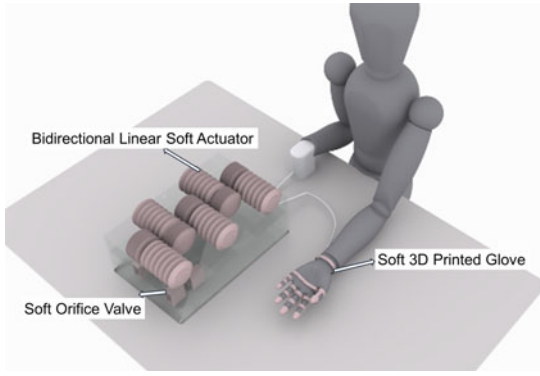


Fig. 1. Conceptual illustration of the proposed soft robotic glove system.

II. CONCEPT AND DESIGN

The proposed glove design was primarily aimed to improve on the following aspects that are essential to the performance and applications of soft robotic gloves in real life:

- 1) *Forces*: Limited force output is a major limitation for existing soft gloves. However it is crucial to ADL functions. Following the biomechanics literature, finger-tip forces of around 10 N [6], [15] per finger should be provided. Better performance was achieved when finger-tip force increased [15], [16].
- 2) *Working pressure*: Although higher pressure naturally leads to higher forces, it will also substantially increase the size, weight, and cost of the pneumatic components required to drive the system. Therefore to maintain compact and lightweight, the working pressure is better below 150 kPa (commercially available micro pumps' maximum pressure);
- 3) *Weight*: The glove piece worn on the hand should be as light as possible to achieve superior ergonomics, and not exceeding the weight of existing soft gloves, which were reported to be around 500 g [6].

Following the design goals, the schematic design of the soft robotic glove is shown in Fig. 2, consisting of three parts: the *soft glove* driven by *BLSAs* through cables, regulated by *SOVs*. The *SOVs* are used for pressure and flow regulation for the desired air pressure P_1 , P_2 into the *BLSA* which then generate the designated motion X_1 , X_2 and actuation forces F_1 , F_2 . With the bidirectional actuation, the glove is capable of flexion and extension motions with variable compliances. Actuation forces transmission to fingertips follow the schematic in Fig. 2, which satisfies

$$F_T = f_T l_1 / l_2 = T_q / l_2, \quad (1)$$

where F_T is the fingertip force, l_2 is the arm length of fingertip force. l_1 is the arm length of cable tension. T_q is the joint torque. Therefore, f_T is the cable tension at the fingertip, which is transmitted from actuation force F_1 . Transmitting efficiency refers to our previous work on the cable-sheath modeling [17], which decreases with the increase of curvature. Therefore, according to (1), fingertip force will be decreased with the flexion of finger.

A. Soft Glove

To ensure the comfort of users' hands, the glove directly contacting with the hands is expected to be both soft and lightweight. In the meantime, the material strength of the soft glove should be sufficient to support the cable transmission for effective actuation. With the advances of 3D printing technology, the entire glove could be 3D-printed using soft and flexible materials for high repeatability and low cost.

Each finger of the glove is driven by two cables at the front and back of finger: one for flexion, the other for extension. Based on the motion pattern of human finger, as the soft glove shown in Fig. 2, the length of yellow line reduces while the length of the other side increases during flexion. In this design, Nodes 1 and 5 are used to fix the tip of cable and sheath, respectively. Nodes 2, 3, 4 located at the middle of two joints are channels for passing cables and fixing the travel route of finger. After the design and modeling work, the glove was 3D-printed (Delta-bot consumer grade 3D-printer) with soft materials (flexible thermoplastic polyurethane (TPU) material, NINJAFLEX, Shore Hardness: 85A). The fabricated prototype of the soft glove is shown in Fig. 3(a). The weight worn on the hand is around 50 g.

B. Bidirectional Linear Soft Actuator

The proposed soft actuator requires high power-to-weight ratio at low working pressure, variable compliance and a special working mechanism for the glove system. As we mentioned, the change of cables length for flexion and extension motions are correlated to each other with simultaneous reduction and increase. Therefore, *BLSA* is required to extend in one direction and contract in the other direction whether for extension or for flexion. The *BLSA* is proposed to consist of two components as indicated in Fig. 2: one is for the actuation generation (bellows), the other is for the motion and force transmission (outer skeleton). Bellow has been chosen as force generation component with its large extension ratio and low actuation pressure. These characteristics are benefitting from both its deformable but un-stretchable material and unique folding structure. Soft bellows are widely adopted in the daily lives as toys, which are factory products with low price and high repeatability of performance. When actuated with compressed air, the bellow will extend. As a result, the top plate will be pushed up. The force f acting on the top plate could be expressed as

$$f = k(x_0 - x) + \pi r^2 P, \quad (2)$$

where k is a stiffness constant depending on the material and structure of the bellow, elaborated in the next section; x is the length of bellow; x_0 is its initial length; p is the inner relative pressure; and r is the effective radius of the bellow. Equation (2) states that the extension force is correlated to the inner pressure and dimensions of the bellow with a linear relation between the force and length, pressure. Besides, the force will increase monotonically as the effective radius of the bellow increases. Larger diameter and initial length lead to larger force and larger travel range, respectively.

An outer skeleton for motion transmission is designed for bellows, as shown in Fig. 2. Pulleys are used at the corners to

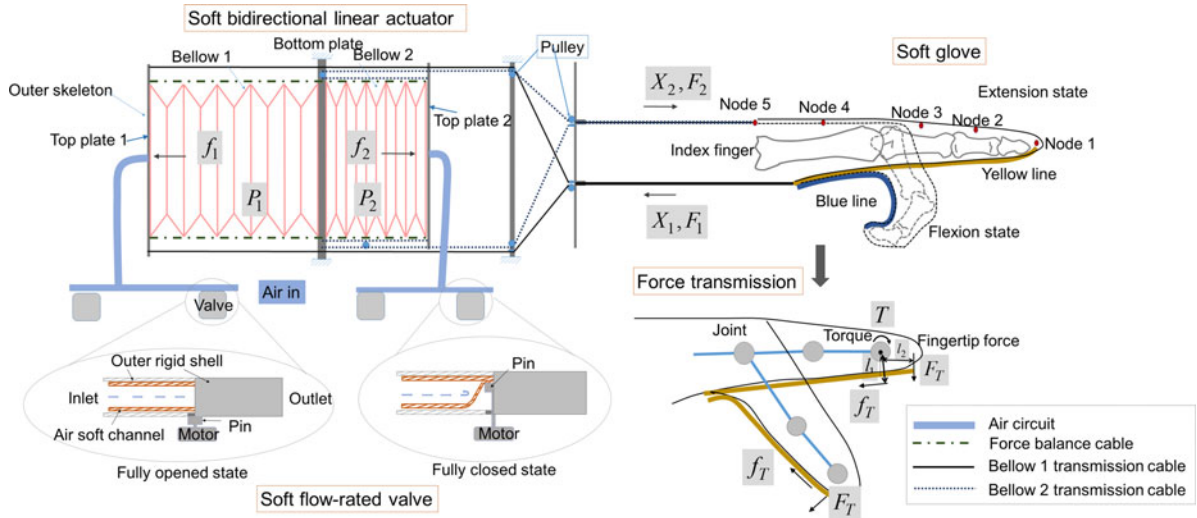


Fig. 2. Schematic of the soft robotic glove. Four sections illustrated: structure illustration of soft glove, force transmission mechanism of glove, and working mechanism of the BLSA and SOV.

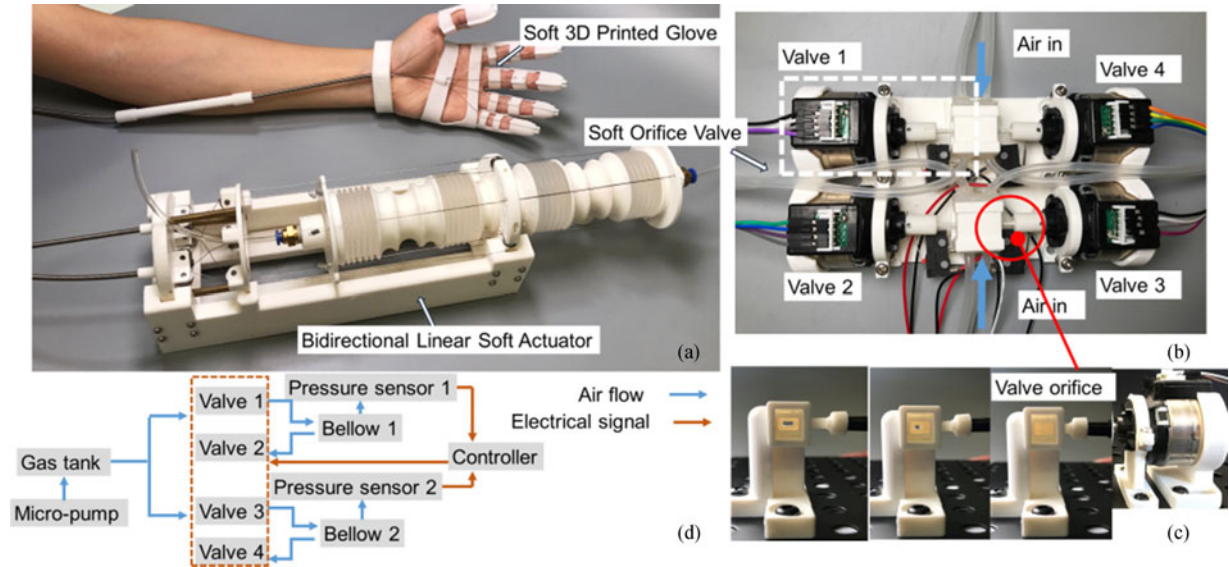


Fig. 3. Prototype of the soft robotic glove system. (a) The soft glove and bidirectional linear soft actuator; (b) Soft orifice valves; (c) Side view of soft orifice valve in three states (from left to right): fully-open, half-open, and fully-close; (d) The pneumatic and electric circuit of the glove system.

change the force direction, therefore, regarding the actuation system, the energy loss in force transmission could be ignored. Forces generated at the top plates could be fully transmitted to the cables. Three types cables are utilized: force balance cable, bellow 1 transmission cable and bellow 2 transmission cable. The bellows transmission cables are used to transmit the motion of bellows independently, while the force balance cable connects these two bellows. The length of force balance cable is constant during operation. Therefore, lengths of Bellow 1 (X_1) and Bellow 2 (X_2) are correlated

$$X_1 + X_2 = 2X_0, \quad (3)$$

where X_0 is the original lengths of Bellow 1 and Bellow 2. As a result,

$$F_1 = 2k(X_0 - X_1) + \pi r^2 (P_1 - P_2), \quad (4)$$

TABLE I
DIMENSIONS OF BLSA AND SOV

Parameter name	Symbol	Dimension
Initial length of Bellow 1(2)	x_0	60 mm
Minimum length of Bellow 1(2)	–	30 mm
Maximum length of Bellow 1(2)	–	90 mm
Effective radius of Bellow 1(2)	r	22 mm
Width of soft orifice	w	4 mm
Height of soft orifice	h	2 mm

Equation (4) will be validated through experiments in Section III.

A prototype of the BLSA with four bellow units (two for Bellow 1 and two for Bellow 2) is shown in Fig. 3(a). Dimensions are listed in Table I.

C. Soft Orifice Valve

Novel soft proportional valves are used to regulate the pressures of BLSA (P_1 , P_2) for proportional air control. The use of proportional valves was to avoid sudden air flux introduced by solenoid valves used in our previous works [6], in order to increase the smoothness of operation, and improve user experience. Commercially available proportional valves are significantly larger, heavier, and costlier than solenoid valves, therefore in this work we attempted to design soft material valves benefiting from the deformability of soft materials. Moreover, conventional proportional valves generally have circular-shape orifices, with nonlinear relations between valve control commands to the resultant air flow rate [18]. With these considerations, the SOV design in this work has a rectangular orifice area. Recent studies on soft gas-tight silicone materials provide the possibility on building soft proportional valve [19]. These soft, deformable materials are capable of working in conditions with large tension.

The concept of the proposed SOV is to proportionally control the orifice area of silicone air channel with a small electric motor. Here the soft air channel could effectively avoid the mechanical contact between components, resulting in a mechanical friction-free working condition. The schematics of the SOV is shown in Fig. 2. The design of SOV consists of two parts: a soft air channel which connects the inlet and outlet of valves, and an electric motor. To proportionally control the orifice area by the motor displacement, a rectangular cross section is adopted for the air channel. The motor drives a square pin indenting laterally and deforms the air channel. The orifice area A is given by

$$A = h(w - x_m), \quad (5)$$

where h is the effective height of air channel, w is the maximum width of the air channel and x_m is the travel displacements of the motor, $x_m = 0$ when the valve is fully opened. In reality, the orifice fabricated from soft silicone material will undergo nonlinear shape deformation, which will be further complicated by the pressure differences between the two ends of the valve. To incorporate the above factors into the above model, a correction term C_p has been introduced to (5),

$$A = h(w + C_p - x_m), \quad (6)$$

where C_p is a coefficient related to the pressure difference between two ends of the valve, and will be determined by calibration experimentally.

Based on the study of the flow through an orifice [18], flow rate through an orifice could be presented as

$$Q = \begin{cases} \frac{C_o A C_1 P_u}{\rho \sqrt{T}} & , \frac{P_d}{P_u} \leq 0.528 \\ \frac{C_o A C_2 P_u}{\rho \sqrt{T}} \left(\frac{P_d}{P_u}\right)^{1/k} \sqrt{1 - \left(\frac{P_d}{P_u}\right)^{(k'-1)/k'}} & , \frac{P_d}{P_u} > 0.528 \end{cases}, \quad (7)$$

where the discharge coefficient of the orifice C_o is an empirical and dimensionless term, it is a could be taken as a constant in most engineering work. The value of C_o will be investigated experimentally in the next section. C_1 and C_2 are constants for a given fluid. P_d , P_u are the downstream and upstream pressures, respectively. T is the upstream stagnation temperature. ρ is the

density of the gas, which is a constant as the air is incompressible in low speed flow [20]. k' is the specific heat ratio. Assuming an adiabatic condition, relations between the flow rate Q and pressure P in a tank with constant volume V is represented as [18]

$$\dot{P} = k' \rho R T (Q_{in} - Q_{out}) / V, \quad (8)$$

where \dot{P} is the time derivative of the tank pressure, R is the ideal gas constant and Q_{in} , Q_{out} are respectively the flow rate flow into and flow out of the tank.

Analyzing (7) and (8), by changing the orifice area of air channel A , pressure could be regulated.

In this glove system, we choose the silicone material (dragon skin 30) and wall thickness of 2 mm for air channel. To linearly deform the wall of soft channel and therefore control the orifice of the air channel, a linear electric motor (Minebea, PL35L-A24) was used. The linear travel displacement of the motor is 10 mm with resolution of 0.016 mm. The SOV assembly is shown in Fig. 3(b), where four soft valves are fabricated for the glove system. Referring to the dimensions of the commercial proportional valve, the air channel is designed with a rectangular cross section (4 mm width, 2 mm height in Table I). The rectangular orifice at fully-open, half-open and fully-close states are presented in Fig. 3(c).

III. EXPERIMENTS

Experiments on the BLSA and the SOV will be presented. After that, the performance of a whole glove system will be evaluated.

A. BLSA Tests

The BLSA consists of two components: force generation (bellows) and force transmission (outer skeleton). Experiments will be conducted on a single bellow first, followed by the assembled BLSA to validate the model (4) in Section II.

1) *Single Bellow Test*: Experimental setup for the single bellow test is shown in Fig. 4(a), where the bellow was mounted on the platform with one end connected to the load cell (range: -100 N ~ 500 N) to measure the extension force following the varying inner pressure p and length x . Pressure and length were changed by a pressure regulator (SMC ITV2030) and a stepper-motor-driven slider, respectively. With this configuration, the $f - x$ relation in isotonic condition and isometric condition were investigated respectively, experimental results are presented in Fig. 4(c) and (d). From the experimental results, extension force proportionally increases with length decreasing and pressure increasing. Results in $p = 0$ kPa was used to calibrate stiffness coefficient $k = 1250$ N/m. Submitting $k = 1250$ N/m back to (2). Modeled results show good agreements with experimental results. Therefore, the value of bellow stiffness is verified, which will be used in the following study.

2) *BLSA Force Test*: Assembled BLSA test were conducted in the platform in Fig. 4(b) to verify the model (4). $F_1 - P_1$ relation was measured in an isometric condition. $P_2 = 10$ kPa was set during the tests. Analyzing the results in Fig. 4(e), $F_1 - P_1$ were recorded fixed in different positions (different

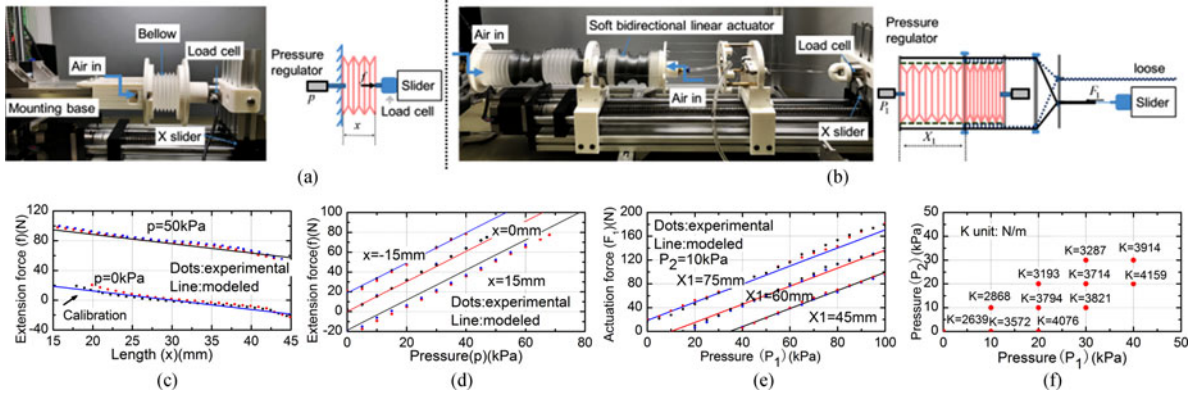


Fig. 4. Actuator tests. (a) Experimental setup for the single bellow test; (b) Experimental setup for bidirectional linear soft actuator; (c) Single bellow test results in isotonic condition (constant $p = 0$ kPa, $p = 50$ kPa, respectively, presented in different color lines), experimental results and modeled results are presented. Here each test was repeated three times (presented in different color dots); (d) Single bellow test results in isometric condition; (e) BLSA test results in isometric condition, experimental results and modeled results are presented; (f) BLSA compliance tests. Here variable stiffness of BLSA in different pressure groups (P_1 , P_2) are presented.

bellow lengths), good agreements between experimental results and modeled results are presented. They demonstrated a good linearity between F_1 and P_1 . The actuator was proved to generate larger force F_1 in larger pressure P_1 and larger bellow extension. When $X_1 = 75$ mm, 180 N actuation force could be generated at an air pressure as low as 100 kPa. The great force capability of this actuator provides superiority when applied to the soft glove system.

3) *BLSA Compliance Test*: A unique feature of the BLSA is its variable compliance which is an ability to adapt the external load with itself body deformation. In our proposed actuator, compliance C is the reciprocal of actuator stiffness K

$$C = K^{-1} = \Delta F_1 / \Delta X_1, \quad (9)$$

where ΔX_1 is length change of Bellow 1 produced by the applied external load differences ΔF_1 .

We tested the variable compliance of BLSA in the platform (Fig. 4(b)). Tests was performed with three steps: 1) charge the Bellow 1 and Bellow 2 to pressure P_1 and P_2 in free space; 2) connect the cable of BLSA to the load cell on the slider; 3) move the slider with displacement $\Delta X_1 = 5$ mm and record the force ΔF_1 read by the load cell. Experimental results are shown in Fig. 4(f) where compliance is expressed by stiffness K . Minimum stiffness is achieved in $P_1 = P_2 = 0$ kPa. It increases with the increase of P_1 and P_2 . Besides, the increase of pressure differences ($P_1 - P_2$) also results an increase of actuator stiffness. Therefore, variable stiffness could be achieved by controlling the inputs of P_1 and P_2 .

B. SOV Tests

To verify the capability of SOV on proportional flow control (model (7)) and pressure regulation, the following two tests were conducted.

1) *Calibration and Validation Test*: Parameters C_0 and C_p in (7) and (6) were determined by calibration. Experimental platform for calibration is shown in Fig. 5(a). In this experimental platform, Q was recorded by the flow sensor (SMC, -3-3LPM).

The orifice area A was controlled by the electric motor with linear displacement x_m . Upstream pressure of the air tank (P_u) was regulated by pressure regulator (SMC, ITV2030, 500 kPa max.). Downstream pressure (P_d) was set to the standard pressure of ambient.

One test was conducted to calibrate C_0 . Analyzing (7), C_0 is the slope of function in a constant $\Delta P' (\Delta P' = P_d - P_u)$. Therefore, $C_0 = 0.14$ was obtained when $\Delta P' = 60$ kPa as in Fig. 5(c). Two more groups of experiments in $\Delta P' = 100$ kPa and $\Delta P' = 160$ kPa were performed to validate the value of C_0 . The experimental and modeled results with good agreements. Therefore, $C_0 = 0.14$ is verified.

The same calibration procedure was followed to obtain C_p , as we mentioned, it is a parameter correlating to $\Delta P'$. Therefore, the relation $\Delta P' - Q$ in constant $x_m = 3$ mm was investigated to calibrate C_p . Experimental results are presented at Fig. 5(d). The estimated $C_p = 0.001 \Delta P'$ was obtained. The other two groups of results verified this value.

These estimated values C_0 and C_p will be used in the following study.

2) *Pressure Regulation Test*: Model (7) was proved to be accurate to describe the relation $x_m - Q$. Therefore, (7), together with (8) were used in modeling of SOV to regulate pressure. Experimental setup for pressure regulation is shown in Fig. 5(b). Hardware of the system includes: two SOVs (one for air in and the other for air out of the bellow (constant volume)), a pressure sensor for monitoring the pressure and a microcontroller (Arduino Uno). A proportional-integral control strategy was applied to control the pressure in the bellow. Controller block diagram is also presented in Fig. 5(b).

Tests were performed by giving a set pressure (50 kPa) to the controller and record the process pressure which was read by the pressure sensor. As Fig. 5(e) shown the SOV set took around 0.2 s to get to the set pressure. The pressure regulation process is proved to be smoother and faster than the solenoid valves regulation [6]. The pressure regulation capability of SOVs was verified and The SOVs could be used in the glove system.

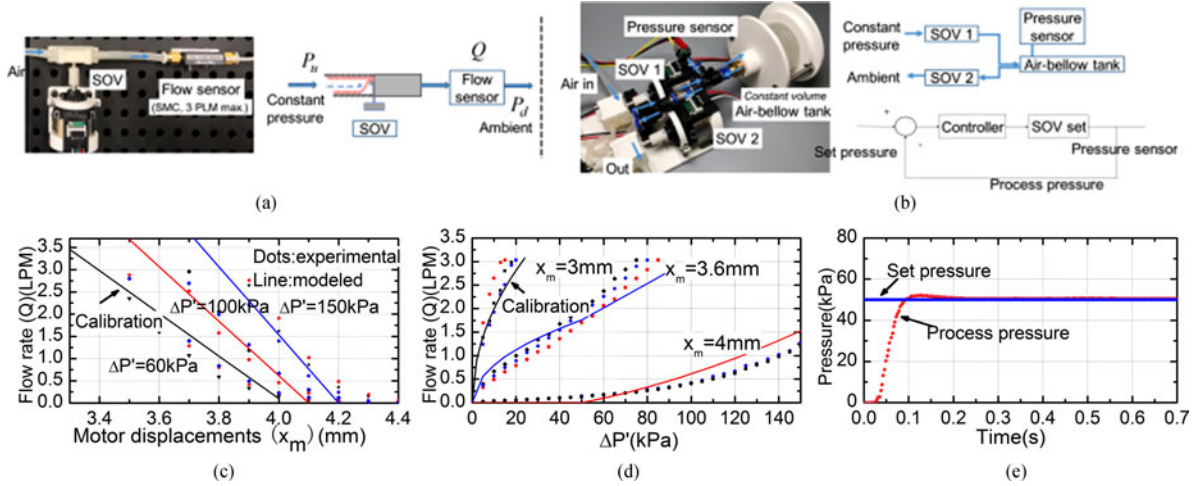


Fig. 5. SOV tests. (a) Experimental setup for soft orifice test; (b) Experimental setup for pressure regulation test and controller block diagram; (c) and (d) Experimental results of soft orifice test; (e) Experimental results of pressure regulation test.

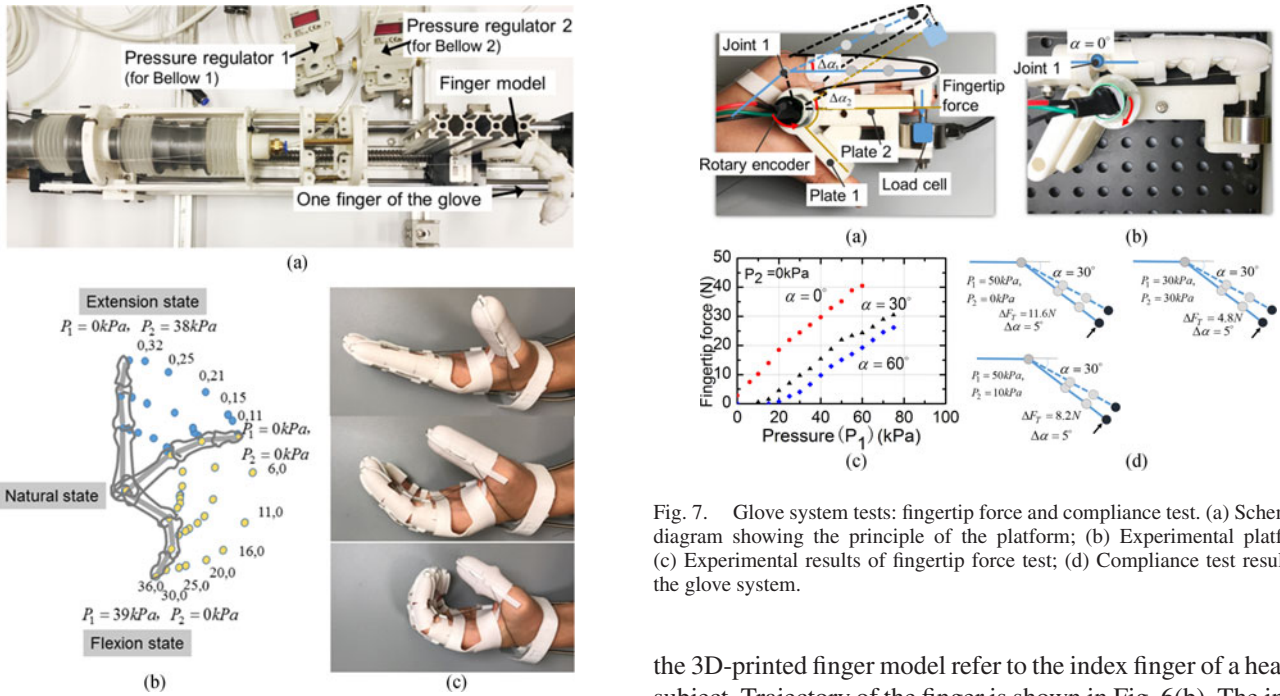


Fig. 6. Glove system test: Motion trajectory in free space. (a) Motion trajectory recording platform; (b) Experimental results: trajectory of index finger in different pressure (P_1 and P_2); (c) Demonstration of glove motion.

C. Glove System Tests

The assembly of the robotic glove system, integrating the actuators and valves with the 3D-printed soft glove. We evaluated the glove system from three aspects: motion trajectory, fingertip force and compliance. As all five fingers are arranged with same motion (flexion and extension), we will take the index finger as a reference.

1) *Motion Trajectory in Free Space*: In the trajectory recording platform (Fig. 6(a)), a camera was used to record a 3D-printed finger model's joints positions in 2D space and two regulators for pressure regulation and recording. Dimensions of

Fig. 7. Glove system tests: fingertip force and compliance test. (a) Schematic diagram showing the principle of the platform; (b) Experimental platform; (c) Experimental results of fingertip force test; (d) Compliance test results of the glove system.

the 3D-printed finger model refer to the index finger of a healthy subject. Trajectory of the finger is shown in Fig. 6(b). The index finger model could be actuated in very low pressure from the natural state to the flexion state ($P_1 = 39 \text{ kPa}$, $P_2 = 0 \text{ kPa}$) and extension state ($P_1 = 0 \text{ kPa}$, $P_2 = 38 \text{ kPa}$).

Photos on motion demonstration are presented in Fig. 6(c), showing the hand motion when wearing the glove. In this demonstration, five fingers were driven by one BLSA.

2) *Fingertip Force Test*: As mentioned, fingertip force is transmitted from actuation force by cables and following the tendency of (1). To investigate this fingertip force, a customized experimental platform (Fig. 7(b)) was developed. Fig. 7(a) was presented to explain the working principle of the platform with same dimensions of finger in the Fig. 7(b). Mechanical structure of the platform includes a rotary joint connects two plates with bearings. Thumb was supported by Plate 1. Index finger was aligned to Plate 2. With this configuration, the rotary angle of platform ($\Delta\alpha_1$) was always kept the same with the rotary

angle of finger joint 1 ($\Delta\alpha_2$). Therefore, the rotation angle of joint 1 could be recorded by the rotary encoder in the platform. Fingertip force could be measured by the load cell.

In the fingertip force test, the pressure-force relationship was recorded in a fixed finger position, i.e., with constant α . α is defined as the angle of joint 1, which equals to zero at the position in Fig. 7(b)). α increases with the joint 1 rotation in clockwise. Experimental results in Fig. 7(c) present the pressure-force relation in $\alpha = 0^\circ, 30^\circ, 60^\circ$ respectively. Fingertip force of 40 N in the air pressure of 60 kPa could be achieved by the robotic glove when $\alpha = 0^\circ$. The force capability of the glove is around five times larger than the Fluid-driven soft-bending robotic gloves [6] with much less actuation pressure. Comparing to the condition $\alpha = 0^\circ$, fingertip force decreases with the increase of α . This tendency matches the prediction in Section II.

3) *Glove Compliance Test*: Compliance of the glove system offer the high safety to users, which benefits from the characteristics of BLSA. As we have mentioned, compliance is defined as an ability to adapt the external load with itself body deformation. The compliance of the glove system here could be described as the joint angle change $\Delta\alpha$ to the external added fingertip force ΔF_T . Test was conducted in the platform in Fig. 7(b). In this test, the Plate 1 and Plate 2 was constrained to one position $\alpha = 30^\circ$. Pressure of Bellow 1 and Bellow 2 (P_1, P_2) were charged to the designated values. The fingertip was applied with an external load, resulting in an angle change of joint 1. Experimental results showing the applied external load and change of the angle joint in three pressure groups are presented in Fig. 7(d). When different P_1, P_2 were applied, the needed external forces (ΔF_T) to make the same deformation of the joint 1 ($\Delta\alpha$) were different. The variable compliance of the glove system could be achieved by controlling the inputs of P_1 and P_2 , which shows agreement with the characteristics of BLSA.

IV. DISCUSSION AND CONCLUSION

A soft robotic glove system with high power-to-weight ratio and superior ergonomics is developed in this study. The design and fabrication of the glove system, including the BLSA actuator and SOV valve were presented in details. The actual soft glove worn by the user was entirely fabricated with flexible material without introducing any rigid joint. Therefore, unlike rigid exoskeletons, the soft glove did not require any alignment of the robot joints with human finger joints. An actuation system, a novel soft actuator BSLA paired with novel valves SOVs, were developed, using cable transmission to synchronize finger actuation for enhanced user comfort. In this letter, we experimentally demonstrate its superior capability in a wide range of applications from rehabilitation, daily assistance, to education and entertainment.

The glove is currently actuated by cable transmission providing flexion and extension for each finger. In future studies, the glove design will be improved to provide more dexterity to the

user. The weight of the whole system will also be decreased. The structure and modeling of the BLSA will be refined to match glove evolutions. Further investigations on the SOV will enable more sophisticated control algorithms for the system to achieve a wider range of functions, paving the way for the soft robotic glove to clinical and real-world applications. Ways of making the designs available publicly will also be considered.

REFERENCES

- [1] E. Cruz, H. Waldinger, and D. Kamper, "Kinetic and kinematic workspaces of the index finger following stroke," *Brain*, vol. 128, no. 5, pp. 1112–1121, 2005.
- [2] G. S. Seale, I. M. Berges, K. J. Ottenbacher, and G. V. Ostir, "Change in positive emotion and recovery of functional status following stroke," *Rehabil. Psychol.*, vol. 55, no. 1, pp. 33–39, 2010.
- [3] M. Fontana, A. Dettori, F. Salsedo, and M. Bergamasco, "Mechanical design of a novel hand exoskeleton for accurate force displaying," in *Proc. 2009 IEEE Int. Conf. Robot. Autom.*, 2009, pp. 1704–1709.
- [4] T. Worsnopp, M. Peshkin, J. Colgate, and D. Kamper, "An actuated finger exoskeleton for hand rehabilitation following stroke," in *Proc. IEEE 10th Int. Conf. Rehabil. Robot.*, 2007, pp. 896–901.
- [5] H. In, B. B. Kang, M. Sin, and K. J. Cho, "Exo-glove: A wearable robot for the hand with a soft tendon routing system," *IEEE Robot. Autom. Mag.*, vol. 22, no. 1, pp. 97–105, Mar. 2015.
- [6] P. Polygerinos, Z. Wang, K. C. Galloway, R. J. Wood, and C. J. Walsh, "Soft robotic glove for combined assistance and at-home rehabilitation," *Robot. Autom. Syst.*, vol. 73, pp. 135–143, 2015.
- [7] Z. Wang, M. Z. Chen, and J. Yi, "Soft robotics for engineers," *HKIE Trans.*, vol. 22, no. 2, pp. 88–97, 2015.
- [8] J. Yi, Z. Shen, C. Song, and Z. Wang, "A soft robotic glove for hand motion assistance," in *Proc. IEEE Int. Conf. Real-Time Comput. Robot.*, 2016, pp. 111–116.
- [9] P. Polygerinos *et al.*, "Modeling of soft fiber-reinforced bending actuators," *IEEE Trans. Robot.*, vol. 31, no. 3, pp. 717–789, Jun. 2015.
- [10] Z. Wang, P. Polygerinos, J. Overvelde, K. Galloway, K. Bertoldi, and C. Walsh, "Interaction forces of soft fiber reinforced bending actuators," *IEEE/ASME Trans. Mechatronics*, vol. 22, no. 2, pp. 717–727, Apr. 2017.
- [11] J. E. Pratt and B. T. Krupp, "Series elastic actuators for legged robots," *Proc. SPIE*, vol. 5422, pp. 135–144, 2004.
- [12] C. Della Santina *et al.*, "The quest for natural machine motion: An open platform to fast-prototyping articulated soft robots," *IEEE Robot. Autom. Mag.*, vol. 24, no. 1, pp. 48–56, Mar. 2017.
- [13] D. P. Holland *et al.*, "The soft robotics toolkit: Strategies for overcoming obstacles to the wide dissemination of soft-robotic hardware," *IEEE Robot. Autom. Mag.*, vol. 24, no. 1, pp. 57–64, Mar. 2017.
- [14] Y. L. Park *et al.*, "Design and control of a bio-inspired soft wearable robotic device for ankle-foot rehabilitation," *Bioinspiration Biomimetics*, vol. 9, no. 1, pp. 1–17, 2014.
- [15] N. Smaby, M. E. Johanson, B. Baker, D. E. Kenney, W. M. Murray, and V. R. Hentz, "Identification of key pinch forces required to complete functional tasks," *J. Rehabil. Res. Dev.*, vol. 41, no. 2, pp. 215–224, 2004.
- [16] K. N. An, E. Y. Chao, W. P. Cooney, and R. L. Linscheid, "Forces in the normal and abnormal hand," *J. Orthopaedic Res.*, vol. 3, no. 2, pp. 202–211, 1985.
- [17] Z. Sun, Z. Wang, and S. J. Phee, "Elongation modeling and compensation for the flexible tendon-sheath system," *IEEE/ASME Trans. Mechatronics*, vol. 19, no. 4, pp. 1243–1250, Aug. 2014.
- [18] E. Richer and Y. Hurmuzlu, "A high performance pneumatic force actuator system: Part I—Nonlinear mathematical model," *Trans. Amer. Soc. Mech. Eng. J. Dyn. Syst. Meas. Control*, vol. 122, no. 3, pp. 416–425, 2000.
- [19] M. Loepfe, C. M. Schumacher, C. H. Burri, and W. J. Stark, "Contrast agent incorporation into silicone enables real-time flow-structure analysis of mammalian vein-inspired soft pumps," *Adv. Funct. Mater.*, vol. 25, no. 14, pp. 2129–2137, 2015.
- [20] J. F. Blackburn, *Fluid Power Control*. Cambridge, MA, USA: MIT Press, 1969.